Characterizing high-energy light curves of Fermi/Lat GRBs

Jarred Gillette

August 21, 2015

Abstract

A systematic analysis of the light curves of Gamma-Ray Burst (GRBs) with redshift and detected at high-energy (> 100 MeV) by Fermi/LAT has never been done before our work, because there were only a handful of detections. Now we have 20 of those, which we can use to characterize the GRBs in their rest frame. We compared a characteristic decay times T_c of GRBs with redshifts using the new "Pass 8" data, and used a Crystal Ball function to parametrize GRB characteristics. An unexpected anti-correlation between T_c and the peak flux was observed. This means that brighter peaked GRBs have shorter durations. There is also no correlation between the T_c and the decay index, which makes the anti-correlation with brightness more clear. This results appears to be consistent with the External Shock model, which is one of the competing hypothesis on the origin of the high-energy emission. We did not observe any bimodality, which is seen in GRBs at lower energies.

1 Introduction

First discovered in the early '60s by accident from satellites monitoring for atomic detonations on Earth [6], Gamma-Ray Bursts are short-lived and violent phenomena. We know that they are related to the death of massive stars, since some have been detected in coincidence with corresponding supernovae[5].

We currently have a model that contains an internal engine, which we do not directly measure, emitting polar jets of particles. This engine may be a black hole in the case of long GRBs, or neutron star mergers for short GRBs [8]. As particles are ejected from the engine they produce internal and external shocks from colliding between each other and the surrounding medium [9].

Internal shocks emit quickly, which is called Prompt Emission. Internal shocks are from faster-moving shells of particles colliding with slower-moving shells in their path, colliding at relativistic speeds, and summing to a total mass ejected of the order of solar masses [9]. Beyond the initial Prompt Emission are External Shocks, as the expelled particles can interact with surrounding medium, and generate another pulse of radiation historically called the Afterglow. Afterglow photons have typically a broader spectrum.

The Fermi Large Area Telescope (LAT) detects ~ 1.3 GRB/month. In this study we characterize the time evolution of the flux for the LAT-detected GRBs with redshift, and we search for correlation with other characteristics of the signal. One such characteristic would be the peak brightness of the GRB. A similar analysis has been done in the past for low energy gamma ray bursts, and a bimodality was discovered that separated short and long GRBs [7]. In the high-energy regime this has never been done before our work, because there were only a handful of detections. Now we have more than a hundred, and 20 of those with redshifts, which we can use to characterize the GRBs in their rest frame.

2 Observations and data

The Fermi satellite was launched to orbit on 2008 June 11. The Gamma-ray Burst Monitor (GBM) and Large Area Telescope (LAT) are its two instruments on board. The GBM covers a the energy range between 10 keV and 10 MeV, and is not used for our purposes. The LAT is a pair production telescope covering an energy range from 20 MeV to ¿300 GeV, although its standard data can be used only above 100 MeV [1]. It features a wide field of view and provides a very good sensitivity for advancing knowledge of GRBs at high energies. The only other telescope covering a similar energy range was the EGRET experiment on board the

SLAC National Accelerator Laboratory, 2575 Sand Hill Road, Menlo Park, CA 94025

This material is based upon work supported by the U.S. Department of Energy, Office of Science, Office of Workforce Development for Teachers and Scientists (WDTS) under the Science Undergraduate Laboratory Internship (SULI) program, under Contract No. DE-AC02-76SF00515.

Transient Name	Redshift
GRB 130702004	0.145
GRB 130427324	0.34
GRB 131231198	0.642
GRB 090328401	0.736
GRB 091003191	0.8969
GRB 090510016	0.903
GRB 091208410	1.0633
GRB 100414097	1.368
GRB 120711115	1.405
GRB 100728095	1.567
GRB 150314205	1.758
GRB 090902462	1.822
GRB 150403913	2.06
GRB 090926181	2.1062
GRB 141028455	2.332
GRB 131108862	2.4
GRB 130518580	2.49
GRB 110731465	2.83
GRB 090323002	3.57
GRB 080916009	4.35

Table 1: List of GRBs used for analysis, as well as redshifts.

Compton Gamma-Ray Observatory (CGRO) [10], which however detected only a handful of GRBs during its 10 year mission.

The first LAT GRB catalog [2] covered the first 3 years of the Fermi mission, and was the first systematic analysis of GRBs in this energy range. It contained 35 detections, and just nine with redshifts. A new detection algorithm was recently announced, increasing detection efficiency by 50 percent from the previous one [11]. We also used a new and better version of the data ("Pass 8", [3]) that was released very recently. Analyzing this new data we have over 100 detected LAT GRBs. We were able to confirm that all but one of the 20 GRBs with measured redshift announced as detections by Fermi had carried over from the previous event analysis version ("Pass 7") to Pass 8. In particular, one GRB from the catalog (GRB 091208410) did not make the significance cut in Pass 8, and was not used in our analysis. For the 19 GRBs in table 1, we had the freedom to transform into the GRB's rest-frame.

3 Methods and analysis

Since some GRBs are fainter than others we need to define a method to measure something related to the duration which we can apply to both bright and faint GRBs. The time at which the GRB falls to a fraction of its peak brightness is a suitable quantity for this. We can also choose the fraction so that the measured quantity is not biased by our detection threshold, which could happen for faint bursts. We chose a fractional value of e^{-1} of the peak brightness, as a natural number, but also a small fractional change that we can measure even for very faint GRBs. We define the time at which the GRB falls to e^{-1} of its peak brightness as the characteristic time (T_c).

Beginning with the recently released Pass 8 data, the following is the analysis process that was followed identically for each trigger within our subset of GRBs. First we performed a likelihood analysis[1] in a broad time interval from the initial trigger time to integrate the detected energy of the GRB. We used this to define time intervals containing each 4 photons with at least 90 percent probability of coming from our point source (as computed by the tool *gtsrcprob*).

We then performed a time resolved likelihood analysis for each time interval. Once each bin had been

[1] fermi.gsfc.nasa.gov/ssc/data/analysis/documentation/Cicerone/Cicerone_Likelihood/Likelihood_overview.html

fitted, we used a so-called Crystal ball function, defined as:

$$C(\mu, \sigma, \gamma, N) = N \cdot \begin{cases} e^{(t-\mu)^2/2\sigma^2}, & t < \mu \\ t^{-\gamma}, & t > \mu \end{cases}, \tag{1}$$

which is a Gaussian with a power-law tail, to model the light curve described by our measurements.

Initially a five dimensional curve, we chose to use a version of the Crystal Ball in which $t_0 = \mu$, i.e., the function immediately transitions to a power law decay after the peak, with no delay. This effectively reduced our parameters to four, while still providing a satisfactory description of the data.

A standard least-square minimization cannot be used to fit our function, because it assumes Gaussian errors and cannot account for the presence of upper limits. Therefore we adopted a different technique based on the Poisson likelihood. Let us consider the Crystal Ball function C in equation 1. The average photon flux from the GRB in the i-th time interval $t_{1,i} - t_{2,i}$, with $i = 1..N_{bins}$, is:

$$F_{pred,i}(\mu, \sigma, \gamma, N) = \frac{1}{t_{2,i} - t_{1,i}} \int_{t_{1,i}}^{t_{2,i}} C(t|\mu, \sigma, \gamma, N)\ dt, \tag{2}$$

which can be solved analytically. The likelihood model in each bin contains a power law model for the spectrum of the GRB plus the background components (Isotropic and Galactic templates, and other sources). Let us divide the parameters contained in the likelihood model for the i-th bin in $(\vec{p}_i, F_{pred,i})$, where $F_{pred,i}$ is the average photon flux for the GRB computed through equation 2 and $\vec{p}_i$ is a vector containing all the other parameters of the likelihood model. We can then write the likelihood for the i-th bin as $L_i = L_i(\mu, \sigma, \gamma, N, \vec{p}_i)$. We treated $\vec{p}_i$ as nuisance parameters, and we maximized the (logarithm of the) *profile* likelihood:

$$\log \widehat{L}(\mu, \sigma, \gamma, N) = \sum_{i=1}^{N_{bins}} \log \max_{\vec{p}_i} \left[L_i\left(\vec{p}_i|\mu, \sigma, \gamma, N\right)\right], \tag{3}$$

obtaining the maximum likelihood estimate for μ, σ, γ, N. Here $\max_{p_i}[L_i(\vec{p}_i|\mu, \sigma, \gamma, N)]$ denotes the maximum of L_i with respect to the $\vec{p}_i$ given μ, σ, γ, N. This technique allows to naturally account for time intervals in which there is no detection, as well as for the size of the time bins.

We accomplished the curve-fitting in two steps. First by using a minimization algorithm, Migrad[2], to maximize the log-likelihood of our four dimensional curve.

We did not stop here because if Migrad cannot constrain all the parameters, which happens for faint bursts, error propagation becomes impossible in calculating T_c. Instead, we decided to use the first estimate provided by Migrad as starting point for a Markov Chain Monte Carlo (MCMC) sampler to further explore the parameter space.

We chose priors for our MCMC which best reflected our assumptions for GRB light curves, given the knowledge coming from the first GRB catalog. We let μ vary between 10^{-3} to 10^3, so that our peak could go close to zero, and out to large peak times. We let γ vary between 0 to 3, which is a conservative choice given that all GRBs in the first GRB catalog have decay indexes between -2 and -1. Finally, we let σ vary between 0 and μ, so as not making a large fraction of the Gaussian in negative time from the detection. We are largely unconcerned with the values of sigma, because our measurement takes place after the peak. We are using the Gaussian only to find when the peak occurs, and when to start the power law decay. Finally we constrain obviously N to stay > 0.

Using the samples provided by the MCMC we are able to measure the distribution of T_c. In particular, we obtained 100k sets of parameters, and calculated T_c for each set. We took the 50th percentile (median) to minimize skewing from outliers, as well as the 32th and the 86th to characterize the width of the distribution. We also took the same percentiles from the distributions of the parameters to plot over our binned light curve for a qualitative check. Such light curves are reported in figure 3-5, where the blue band encloses the central 68% of the flux distribution and the green band represents the 95%.

Finally we divided T_c by $1 + z$, where z is redshift, to transform into the rest frame. We then compared the time of e^{-1} of the peak brightness against the peak brightness itself to identify any correlation between these two characteristic parameters of a GRB.

[2]http://seal.web.cern.ch/seal/work-packages/mathlibs/minuit/index.html

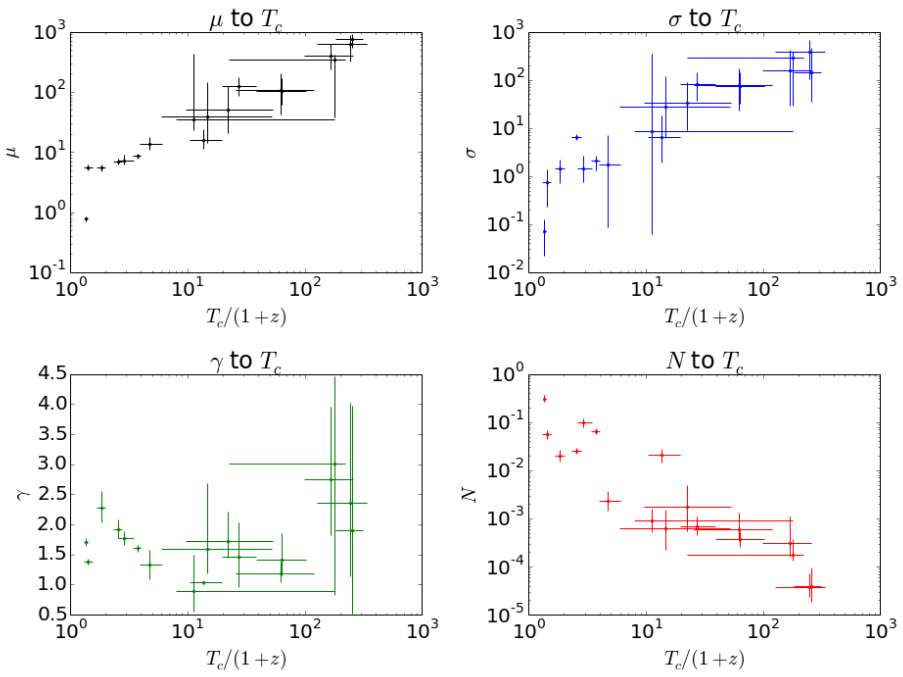

Figure 1: Measurements for the Crystal Ball parameters compared with the characteristic time T_c corrected for cosmological time dilation.

4 Results

After comparing our 19 GRB characteristic times with their respective features the resulting plot (Figure 1) showed a correlation, and anti-correlation, between several parameters. We plotted $T_c/(1+z)$ against each parameter of our function, μ, σ, γ, and N. There is little to no correlation between T_c and decay index, and there is anti-correlation between T_c and the peak flux.

5 Discussion

Correlation was expected between the characteristic time and the time of the peak GRB brightness, as well as the width of the Gaussian. Since T_c cannot happen before the peak we expect its value to increase as the peak brightness occurs later, which also widens the Gaussian. This is confirmed in our plot of 19 GRBs with redshift corrected T_c (figure 1). The more interesting characteristics begin at the peak. The anti-correlation between T_c and the peak flux (bottom right panel) was unexpected, and somewhat counter-intuitive. This means that brighter peaked GRBs have shorter durations. There is also no apparent correlation between T_c and decay index (bottom left panel), which makes the anti-correlation with brightness more clear. Another related anti-correlation is found by plotting the peak luminosity against the time of the peak corrected for the redshift ($\mu/(1+z)$), as shown in figure 2. These anti-correlations agree with what expected from an External Shock interpretation of the LAT emission, where bright GRBs have larger Lorentz Factors than faint GRBs [4]. We did not observe any bimodality, which has been seen in lower energy GRBs.

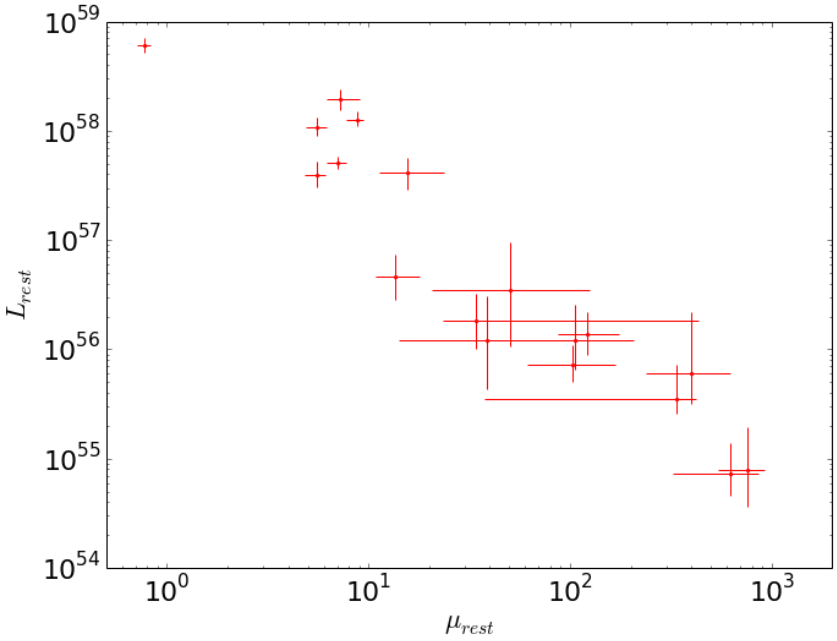

Figure 2: Luminosity of the GRB versus the time of peak brightness, both in the rest frame of the GRB.

6 Acknowledgements

Mentors:
Giacomo Vianello
Nicola Omodei

This work was supported in part by the U.S. Department of Energy, Office of Science, Office of Workforce Development for Teachers and Scientists (WDTS) under the Science Undergraduate Laboratory Internships Program (SULI).

References

[1] M. Ackermann, M. Ajello, A. Albert, and et.al. The Fermi Large Area Telescope on Orbit: Event Classification, Instrument Response Functions, and Calibration. ApJS, 203:4, November 2012.

[2] M. Ackermann, M. Ajello, K. Asano, and et.al. The First Fermi-LAT Gamma-Ray Burst Catalog. ApJS, 209:11, November 2013.

[3] W. Atwood, A. Albert, L. Baldini, M. Tinivella, J. Bregeon, M. Pesce-Rollins, C. Sgrò, P. Bruel, E. Charles, A. Drlica-Wagner, A. Franckowiak, T. Jogler, L. Rochester, T. Usher, M. Wood, J. Cohen-Tanugi, and S. Zimmer for the Fermi-LAT Collaboration. Pass 8: Toward the Full Realization of the Fermi-LAT Scientific Potential. *ArXiv e-prints*, March 2013.

[4] G. Ghisellini, G. Ghirlanda, L. Nava, and A. Celotti. GeV emission from gamma-ray bursts: a radiative fireball? MNRAS, 403:926–937, April 2010.

[5] J. Hjorth. The supernova-gamma-ray burst-jet connection. *Royal Society of London Philosophical Transactions Series A*, 371:20275, April 2013.

[6] R. W. Klebesadel, I. B. Strong, and R. A. Olson. Observations of Gamma-Ray Bursts of Cosmic Origin. ApJ, 182:L85, June 1973.

[7] C. Kouveliotou, C. A. Meegan, G. J. Fishman, N. P. Bhat, M. S. Briggs, T. M. Koshut, W. S. Paciesas, and G. N. Pendleton. Identification of two classes of gamma-ray bursts. ApJ, 413:L101–L104, August 1993.

[8] A. I. MacFadyen, S. E. Woosley, and A. Heger. Supernovae, Jets, and Collapsars. ApJ, 550:410–425, March 2001.

[9] T. Piran. Gamma-ray bursts and the fireball model. Phys. Rep., 314:575–667, June 1999.

[10] D. J. Thompson, D. L. Bertsch, C. E. Fichtel, R. C. Hartman, R. Hofstadter, E. B. Hughes, S. D. Hunter, B. W. Hughlock, G. Kanbach, D. A. Kniffen, Y. C. Lin, J. R. Mattox, H. A. Mayer-Hasselwander, C. von Montigny, P. L. Nolan, H. I. Nel, K. Pinkau, H. Rothermel, E. J. Schneid, M. Sommer, P. Sreekumar, D. Tieger, and A. H. Walker. Calibration of the Energetic Gamma-Ray Experiment Telescope (EGRET) for the Compton Gamma-Ray Observatory. ApJS, 86:629–656, June 1993.

[11] G. Vianello, N. Omodei, and Fermi/LAT collaboration. The First 100 LAT Gamma-Ray Bursts: A New Detection Algorithm and Pass 8. *ArXiv e-prints*, February 2015.

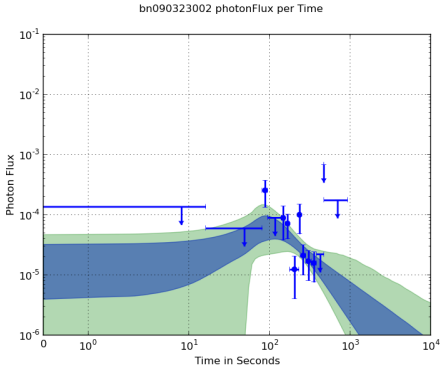

(a) GRB 090323002.

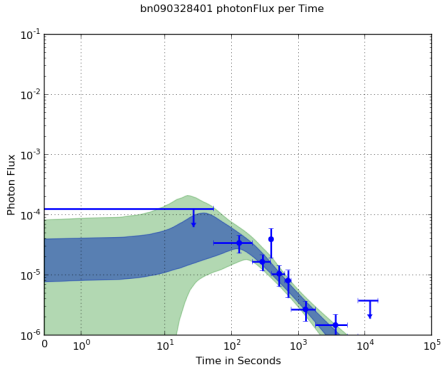

(b) GRB 090328401.

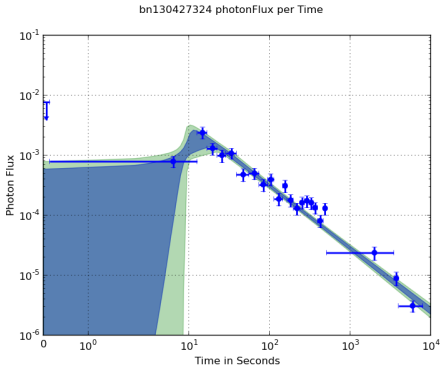

(c) GRB 130427324.

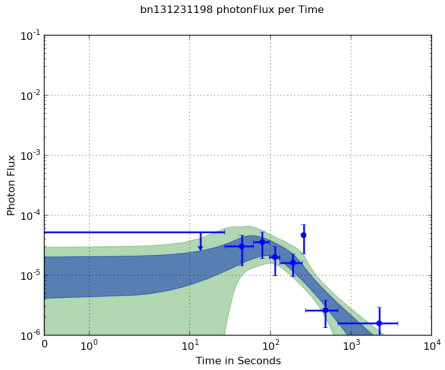

(d) GRB 131231198.

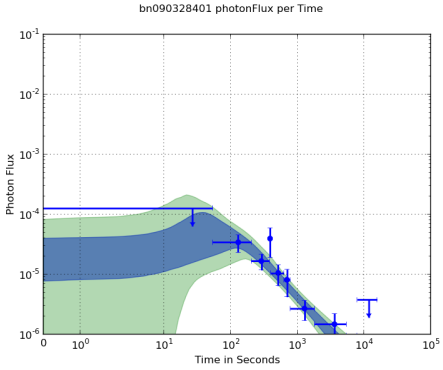

(e) GRB 090328401.

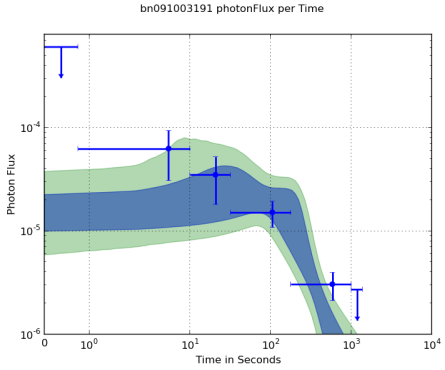

(f) GRB 091003191.

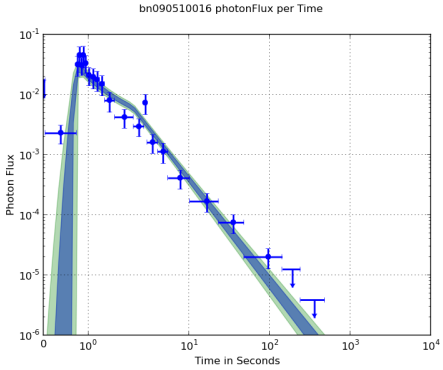

(g) GRB 090510016.

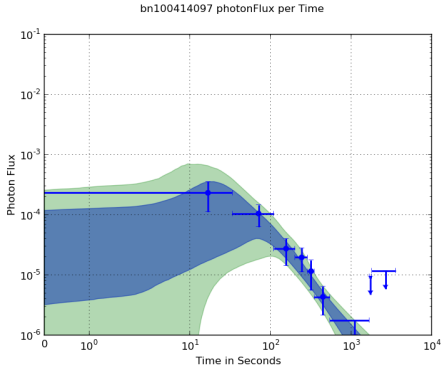

(h) GRB 100414097.

Figure 3: Plots of Fitted Light Curves. The blue band encloses the central 68% of the flux distribution and the green band represents the 95%.

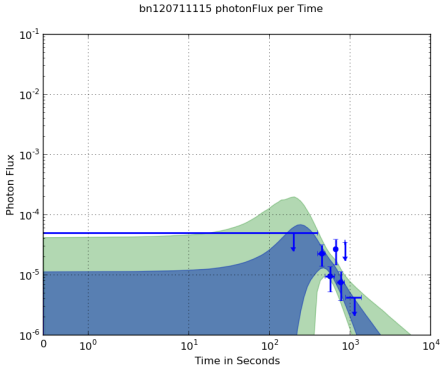

(a) GRB 120711115.

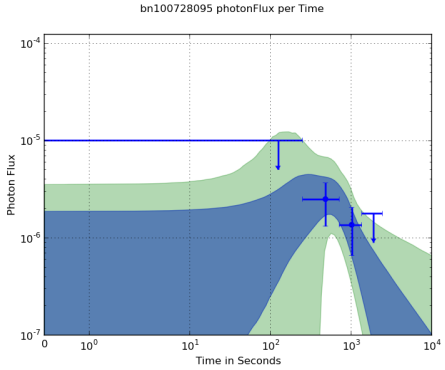

(b) GRB 100728095.

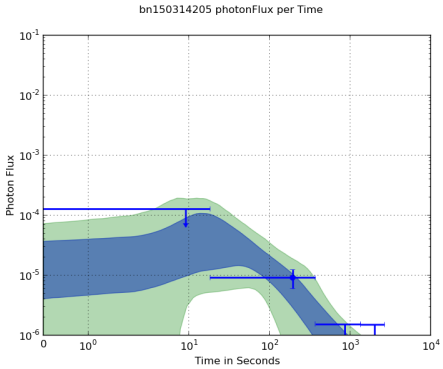

(c) GRB 150314205.

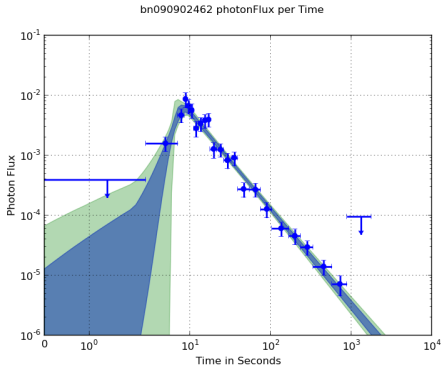

(d) GRB 090902462.

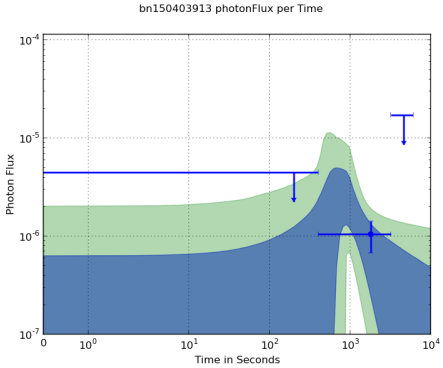

(e) GRB 150403913.

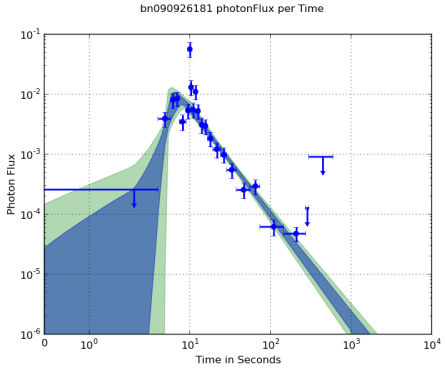

(f) GRB 090926181.

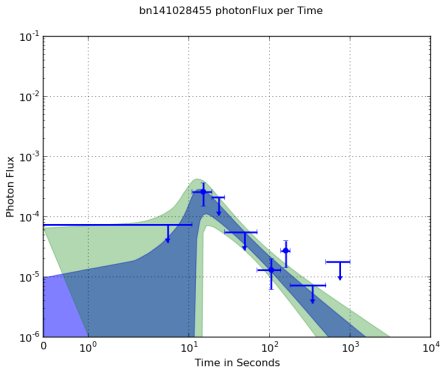

(g) GRB 141028455.

Figure 4: Plots of Fitted Light Curves cont.

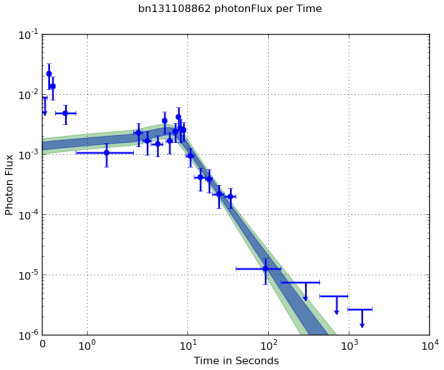

(a) GRB 131108862.

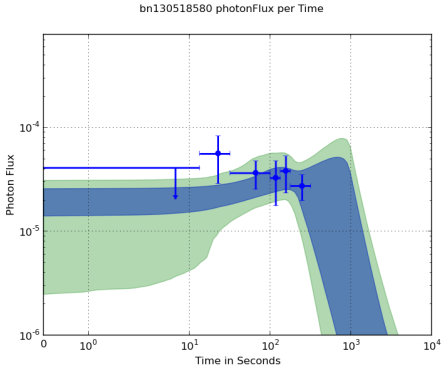

(b) GRB 130518580.

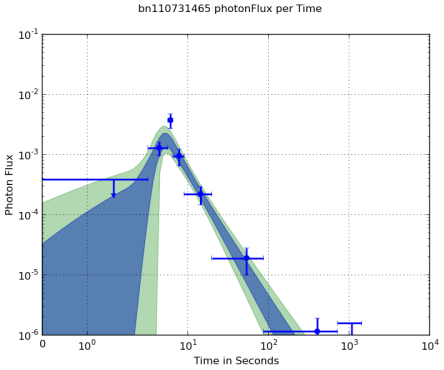

(c) GRB 110731465.

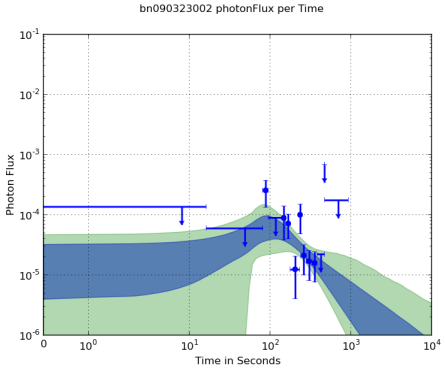

(d) GRB 090323002.

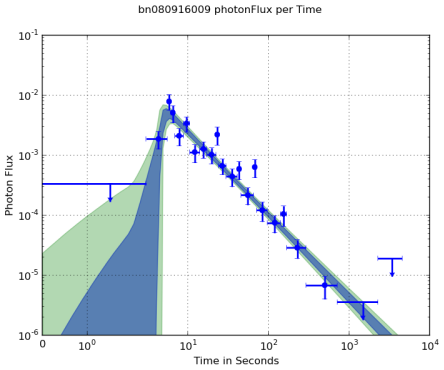

(e) GRB 080916009.

Figure 5: Plots of Fitted Light Curves cont.